# Dynamic long range interaction induced topological edge modes in dispersive gyromagnetic lattices

Raymond P. H. Wu,[1] Yongliang Zhang,[1] K. F. Lee,[1] Jin Wang,[1,2] S. F. Yu,[1] and Kin Hung Fung[1,*]
[1]*Department of Applied Physics, The Hong Kong Polytechnic University, Hung Hom, Kowloon, Hong Kong*
[2]*School of Physics, Southeast University, Nanjing 211189, China*

(Received 17 December 2018; published 24 June 2019)

We study the dynamic long range interaction induced topological photonic bands and edge modes in a one-dimensional (1D) array of strongly dispersive gyromagnetic resonant cylinders. We propose a 1D topological model for such a dispersive gyromagnetic system and demonstrate that the dynamic long-range interaction can lead to localized topological edge modes, while the quasistatic interaction alone does not. Different from the conventional Su-Schrieffer-Heeger model that has only nearest-neighbor interactions, we find that the normal modes of the system coupled strongly to the photon mode of the background medium and the dynamic effects create a different band gap. Our results indicate the importance of the dynamic long-range interactions on the band structures and topological edge modes in strongly dispersive gyromagnetic systems.

DOI: 10.1103/PhysRevB.99.214433

## I. INTRODUCTION

In the past decade, topological photonics [1,2] has become a rapidly growing field of research since the analogs of quantum Hall edge states were theoretically proposed [3–5] and experimentally realized [6] in two-dimensional (2D) gyromagnetic photonic crystals. The bulk-boundary correspondence predicts edge modes existing at the boundary between systems with distinct topological phases, which are backscattering-immune and robust against local perturbations [1,2]. Topological edge modes can be supported in many photonic systems, such as coupled resonator arrays [7–9], bi-anisotropic metamaterials [10], photonic crystals made of dielectric cylinders [11], radiofrequency circuits [12], cavity and circuit quantum electrodynamics systems [13,14], and three-dimensional Weyl points and nodal lines systems [15], or in even higher synthetic dimensions [16,17]. The enhanced light-matter interactions associated with topological edge modes may lead to many potential applications, such as efficient and robust lasers [18–23].

Recently, it has been shown that topological modes can be realized in one-dimensional (1D) photonic crystals [24,25] and 1D arrays of plasmonic [26–32] and dielectric nanoparticles [33–35]. In particular, the Majorana states are found in the zigzag chains of plasmonic nanoparticles [26], and lasing topological edge states are reported in the photonic analogs of the Su-Schrieffer-Heeger (SSH) model [18,20,21]. The SSH model [36] describing electrons in a 1D lattice with staggered hopping is one of the simplest systems exhibiting nontrivial topological bands, which has stimulated a variety of efforts to search for robust topological modes in different photonic structures. In the SSH model, the chiral symmetry ensures the spectral position of the edge state lies at the zero-energy state associated with the isolated site, and the band structure is symmetric with respect to it [37]. This was validated in a variety of analogous photonic systems under the tight-binding approach [27,33,35].

In the present work, we investigate the effects of dynamic long-range interactions on the photonic band structures and the topological edge modes in 1D arrays of dispersive gyromagnetic resonators beyond the SSH model. We use the eigenresponse theory [38–41], which was extensively used in the studying of coupled plasmonic resonators, to account for the dynamic long-range interactions and, meanwhile, to create mapping to a non-Hermitian eigenvalue problem. The electromagnetic resonances of gyromagnetic lattices are then studied. We found that the normal modes of the system coupled strongly to the photon mode of the background medium. The dynamic long-range interaction plays a crucial role in opening a band gap and supporting the topological edge modes in the dimer lattices, which is in contrast with the conventional SSH systems, such as in arrays of plasmonic [27,29] and in dielectric nanoparticles [33,35]. Using a dipole model, the topological phase transition associated with band inversion [42] is illustrated. We demonstrated that the dynamic long-range interactions lead to localized topological edge modes, which is different from the SSH model and cannot be predicted with a tight-binding approach with only short-range interactions being considered. Because chiral symmetry of the system is broken due to the dynamic long-range interactions, the topological edge modes redshifted from the zero-energy mode associated with a single resonator, and the band structures are not symmetric with respect to it. Our results indicate the importance of the dynamic long-range interactions on the band structure and topological edge modes in gyromagnetic systems, and they deepen our understanding of the topology in nonreciprocal photonic systems.

This article is organized as follows. In Sec. II, we describe the coupled-dipole method and introduce the eigenresponse theory by considering a regular chain of dispersive gyromagnetic cylinders. In Sec. III, we illustrate the formation of nontrivial band gaps in a dimerized chain, and we demonstrate topological edge modes supporting in a finite lattice.

*khfung@polyu.edu.hk

 

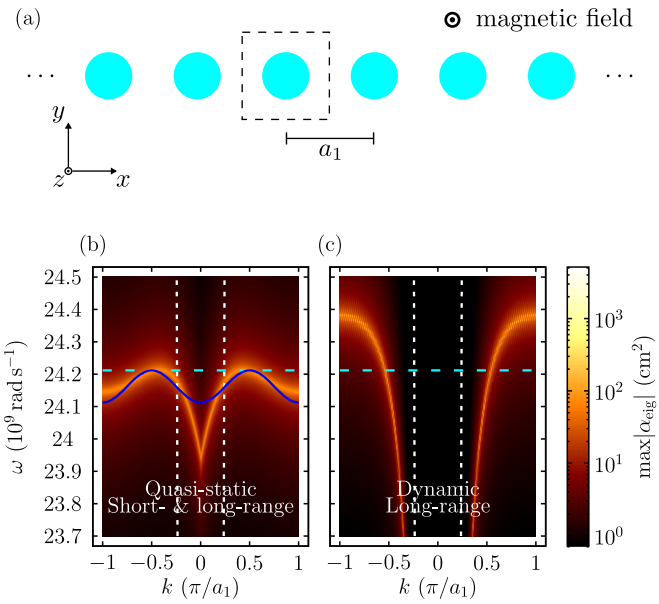


FIG. 1. (a) Illustration of gyromagnetic cylinders on a 1D infinite lattice. The lattice constant is given by $a_1$. The unit cell is indicated by the dashed box. (b) The photonic band structure with short- and long-range interactions in the quasistatic limit. The blue line is the dispersion relation with nearest-neighbor interactions only. (c) The photonic band structure with dynamic long-range interactions. The white dotted lines are the light lines, and the region within the light lines is the light cone. The cyan dashed line indicates the resonant frequency of a single gyromagnetic cylinder $\omega_0$.

## II. REGULAR CHAIN

### A. Coupled-dipole method

We begin by considering a 1D lattice with lattice constant $a_1 = 9.375$ mm in the $x$ direction as depicted in Fig. 1(a). The unit cell consists of one gyromagnetic cylinder with radius $r = 2.5$ mm and the axis of the cylinder in the $z$ direction. The parameters are chosen with $a_1 \geqslant 3r$, such that the cylinders are not too close to each other. For frequencies near the dipole resonance, we take the dipole approximation, in which each cylinder is treated as a point dipole [43]. We are interested in the fields perpendicular to the axis of the cylinder in the $xy$ plane. A magnetic dipole moment $\boldsymbol{m}(\boldsymbol{\rho}) = \boldsymbol{\alpha}(\omega)\boldsymbol{B}(\boldsymbol{\rho})$ will be induced when the cylinder at $\boldsymbol{\rho}$ is in a magnetic field $\boldsymbol{B}(\boldsymbol{\rho})$, where $\boldsymbol{\alpha}(\omega)$ is the polarizability of the cylinder. The polarizability of a cylinder is given by [44]

$$\boldsymbol{\alpha}^{-1}(\omega) = \frac{4\pi}{A}([\boldsymbol{\mu}(\omega) - \boldsymbol{I}]^{-1} + \boldsymbol{L}) - i\frac{\pi k_0^2}{2}\boldsymbol{I}, \tag{1}$$

where $A = \pi r^2$, $\boldsymbol{I}$ is the $2 \times 2$ identity matrix, $\boldsymbol{L} = (1/2)\boldsymbol{I}$ is the demagnetization factors for the cylinder, $k_0 = \omega/c$ is the wave number in the background medium, and $\boldsymbol{\mu}(\omega)$ is the permeability tensor of the gyromagnetic medium. The radiative correction term $-i(\pi k_0^2/2)\boldsymbol{I}$ is included to satisfy the optical theorem. For the case in which the applied static magnetic field $\boldsymbol{H}$ and the saturation magnetization $\boldsymbol{M}$ are parallel to the axis of the cylinder in the $+z$ direction, the permeability tensor is given by [45]

$$\boldsymbol{\mu}(\omega) = \begin{pmatrix} \mu_1 & -i\mu_2 \\ i\mu_2 & \mu_1 \end{pmatrix}, \tag{2}$$

with

$$\mu_1 = 1 + \frac{\omega_m(\omega_h - i\beta\omega)}{(\omega_h - i\beta\omega)^2 - \omega^2}, \tag{3a}$$

$$\mu_2 = \frac{\omega_m\omega}{(\omega_h - i\beta\omega)^2 - \omega^2}, \tag{3b}$$

where $\omega_h = \gamma H$ and $\omega_m = \gamma 4\pi M$, in which $\gamma$ is the gyromagnetic ratio and $\beta$ is the damping factor. We consider that the cylinders are made of yttrium iron garnet (YIG), which is a ferrimagnetic material with very low loss. The parameters for YIG are $H = 500$ Oe, $4\pi M = 1750$ G [46,47], and $\beta = 3 \times 10^{-4}$ [48]. From these expressions, we have

$$\boldsymbol{\alpha}^{-1}(\omega) = \begin{pmatrix} \frac{4}{r^2}\left(\frac{\omega_h}{\omega_m} + \frac{1}{2} - i\beta\frac{\omega}{\omega_m}\right) - i\frac{\pi k_0^2}{2} & i\frac{4}{r^2}\left(\frac{\omega}{\omega_m}\right) \\ -i\frac{4}{r^2}\left(\frac{\omega}{\omega_m}\right) & \frac{4}{r^2}\left(\frac{\omega_h}{\omega_m} + \frac{1}{2} - i\beta\frac{\omega}{\omega_m}\right) - i\frac{\pi k_0^2}{2} \end{pmatrix}. \tag{4}$$

The resonant frequency of a single gyromagnetic cylinder $\omega_0$ is found by solving $\mathrm{Re}[\det \boldsymbol{\alpha}^{-1}(\omega_0)] = 0$, which gives

$$\omega_0 = \omega_h + \frac{\omega_m}{2}. \tag{5}$$

It is equal to $f_0 = \omega_0/(2\pi) = 3.853$ GHz, which is in the microwave regime. $\omega_0$ can be interpreted as the spectral position of the zero-energy state in the SSH model.

The field at $\boldsymbol{\rho}$ due to the induced dipole moment at $\boldsymbol{\rho}'$ is given by $\boldsymbol{B}(\boldsymbol{\rho}) = 4\pi k_0^2 \boldsymbol{G}(\boldsymbol{\rho}, \boldsymbol{\rho}')\boldsymbol{m}(\boldsymbol{\rho}')$ [49], where $\boldsymbol{G}(\boldsymbol{\rho}, \boldsymbol{\rho}')$ is the 2D Green's tensor. For our system, we have [50]

$$\boldsymbol{G}(\boldsymbol{\rho}, \boldsymbol{\rho}') = \begin{pmatrix} G_{xx} & 0 \\ 0 & G_{yy} \end{pmatrix}, \tag{6}$$

with

$$G_{xx} = \frac{i}{4}\left(\frac{1}{k_0 R}\right)H_1^{(1)}(k_0 R), \tag{7a}$$

$$G_{yy} = \frac{i}{4}\left(H_0^{(1)}(k_0 R) - \frac{1}{k_0 R}H_1^{(1)}(k_0 R)\right), \tag{7b}$$

where $\boldsymbol{R} := \boldsymbol{\rho}' - \boldsymbol{\rho}$ is the relative displacement between the source and the observation points, and $H_i^{(1)}$ is the Hankel function of the first kind. In the quasistatic limit $k_0 \to 0$, the field varies inversely as the square of the distance $B \sim 1/R^2$ (see Appendix A). For an array of cylinders, the local field at a dipole is given by the sum of the external field and the

fields from all the other dipoles. The dipole-dipole interaction between cylinders leads to the following coupled-dipole equations:

$$\boldsymbol{m}(\boldsymbol{\rho}) = \boldsymbol{\alpha}(\omega)\left(4\pi k_0^2 \sum_{\boldsymbol{\rho}'\neq\boldsymbol{\rho}} \boldsymbol{G}(\boldsymbol{\rho},\boldsymbol{\rho}')\boldsymbol{m}(\boldsymbol{\rho}') + \boldsymbol{B}_0(\boldsymbol{\rho})\right), \quad (8)$$

where the sum includes all the dipole moments except the self-interaction term, and $\boldsymbol{B}_0(\boldsymbol{\rho})$ is the external excitation magnetic field. For example, $\boldsymbol{B}_0$ can be the field of a plane wave.

### B. Eigenresponse theory

Instead of solving Eq. (8) directly, which involves numerical complex root-finding, we use an eigenresponse theory to study the spectral response of the system. To do so, we define

$$\boldsymbol{M}(\omega) := \boldsymbol{\alpha}^{-1}(\omega) - 4\pi k_0^2 \sum_{\boldsymbol{\rho}'\neq\boldsymbol{\rho}} \boldsymbol{G}(\boldsymbol{\rho},\boldsymbol{\rho}'). \quad (9)$$

For a system with $N$ gyromagnetic cylinders, $\boldsymbol{M}(\omega)$ is a $2N \times 2N$ matrix. Then Eq. (8) can be rewritten as

$$\boldsymbol{M}(\omega)\boldsymbol{m} = \boldsymbol{B}_0. \quad (10)$$

This relates the dipole moments $\boldsymbol{m}$ with the external excitation field $\boldsymbol{B}_0$. In the eigenresponse theory [38–41], which is based on spectral decomposition, we consider the eigenvalue problem

$$\boldsymbol{M}(\omega)\boldsymbol{m}_i = \lambda_i(\omega)\boldsymbol{m}_i, \quad (11)$$

where $\lambda_i(\omega)$ is the eigenvalue corresponding to the eigenmode $\boldsymbol{m}_i$. We define the quantity

$$\alpha_{\text{eig}} := \frac{1}{\lambda} \quad (12)$$

as the eigenpolarizability, which has the dimension $\text{cm}^2$, the same as that of the polarizability $\boldsymbol{\alpha}$. The eigenpolarizability can be interpreted as the response function of the corresponding eigenmode for an external excitation field, and the peaks of $\text{Im}(\alpha_{\text{eig}})$ represent resonances.

For a 1D infinite lattice, the translational symmetry leads to Bloch's theorem,

$$\boldsymbol{m}(\boldsymbol{\rho}+\boldsymbol{R}) = e^{i\boldsymbol{k}\cdot\boldsymbol{R}}\boldsymbol{m}(\boldsymbol{\rho}), \quad (13)$$

where the displacement $\boldsymbol{R} = na_1\hat{x}$, with integer $n$ and lattice constant $a_1$, and the wave vector $\boldsymbol{k} = k\hat{x}$, with the first Brillouin zone $k \in [-\pi/a_1, \pi/a_1]$. Also, we have $\boldsymbol{G}(\boldsymbol{\rho},\boldsymbol{\rho}') = \boldsymbol{G}(0,\boldsymbol{R})$. The coupled-dipole equation for an infinite lattice is given by

$$\boldsymbol{m}(\boldsymbol{\rho}) = \boldsymbol{\alpha}(\omega)\left(4\pi k_0^2 \sum_{\boldsymbol{R}\neq 0} \boldsymbol{G}(0,\boldsymbol{R})e^{i\boldsymbol{k}\cdot\boldsymbol{R}}\boldsymbol{m}(\boldsymbol{\rho}) + \boldsymbol{B}_0(\boldsymbol{\rho})\right), \quad (14)$$

and we define

$$\boldsymbol{M}(\boldsymbol{k},\omega) := \boldsymbol{\alpha}^{-1}(\omega) - 4\pi k_0^2 \sum_{\boldsymbol{R}\neq 0} \boldsymbol{G}(0,\boldsymbol{R})e^{i\boldsymbol{k}\cdot\boldsymbol{R}}. \quad (15)$$

The translational symmetry reduces $\boldsymbol{M}$ to a $2\times 2$ matrix. Then Eq. (14) can be rewritten as

$$\boldsymbol{M}(\boldsymbol{k},\omega)\boldsymbol{m} = \boldsymbol{B}_0. \quad (16)$$

Then the eigenvalue problem for an infinite lattice is

$$\boldsymbol{M}(\boldsymbol{k},\omega)\boldsymbol{m}_i = \lambda_i(\boldsymbol{k},\omega)\boldsymbol{m}_i. \quad (17)$$

It should be noted that $\boldsymbol{M}$ is non-Hermitian due to the loss and dynamic effects. From now on, we set $\boldsymbol{B}_0 = \boldsymbol{0}$ so as to study the normal modes of the system.

### C. Infinite lattice

#### 1. *Quasistatic limit*

We calculate the band structure of the gyromagnetic system described in Sec. II A in an infinite lattice. Before studying the more general case, we consider the system in the quasistatic limit $k_0 \to 0$. The coupled-dipole equations in the quasistatic limit are described in Appendix A. From Eq. (A10), we have

$$\boldsymbol{M}'(\boldsymbol{k},\omega) = \begin{pmatrix} \frac{4}{r^2}\left(\frac{\omega_h}{\omega_m}+\frac{1}{2}-i\beta\frac{\omega}{\omega_m}\right) - \sum_{\boldsymbol{R}\neq\boldsymbol{0}}\frac{2}{R^2}e^{i\boldsymbol{k}\cdot\boldsymbol{R}} & i\frac{4}{r^2}\left(\frac{\omega}{\omega_m}\right) \\ -i\frac{4}{r^2}\left(\frac{\omega}{\omega_m}\right) & \frac{4}{r^2}\left(\frac{\omega_h}{\omega_m}+\frac{1}{2}-i\beta\frac{\omega}{\omega_m}\right) + \sum_{\boldsymbol{R}\neq\boldsymbol{0}}\frac{2}{R^2}e^{i\boldsymbol{k}\cdot\boldsymbol{R}} \end{pmatrix}. \quad (18)$$

Then, the system is described by

$$\boldsymbol{M}'(\boldsymbol{k},\omega)\boldsymbol{m} = \boldsymbol{0}. \quad (19)$$

Now, we take the tight-binding approach, in which only short-range interactions are being considered. By including only the nearest-neighbor interactions, the dispersion relation and the normal mode can be obtained analytically by solving the nontrivial solution of Eq. (19). From $\text{Re}[\det \boldsymbol{M}'(\boldsymbol{k},\omega)] = \boldsymbol{0}$, we obtain the dispersion relation

$$\omega(k) = \omega_0\sqrt{1-f(k)^2}, \quad (20)$$

with

$$f(k) := \left(\frac{r}{a_1}\right)^2 \frac{\omega_m}{\omega_0}\cos(ka_1). \quad (21)$$

It is plotted with a blue line in Fig. 1(b). We observe a single narrowband. The normal mode of the system does not couple to the photon mode of the background medium. At $k = \pm\pi/(2a_1)$, the resonant frequency of the system is equal to that of a single gyromagnetic cylinder $\omega_0$, while at other $k$, the band is below $\omega_0$. The group velocity $v_g = d\omega/dk$ of the normal mode is zero, $v_g = 0$, at $k = 0, \pm\pi/(2a_1), \pm\pi/a_1$.

We will soon show that the results obtained in the quasistatic limit do not correctly describe the qualitative features of the system. Nevertheless, we see that only one nontrivial solution is obtained from the $2 \times 2$ matrix problem of Eq. (19). The normalized normal mode is given by

$$\boldsymbol{m} = \frac{1}{\sqrt{2}} \begin{pmatrix} \sqrt{1+f(k)}e^{-i\frac{\pi}{2}} \\ \sqrt{1-f(k)} \end{pmatrix}. \tag{22}$$

We find that the longitudinal mode and the transverse mode are coupled, such that the magnetic dipole moments rotate counterclockwise elliptically. This is different from the analogous plasmonic system, where two nontrivial solutions, which correspond to the longitudinal mode and the transverse mode, will be obtained.

#### 2. Dynamic long-range interaction

Now, we extend our calculation to include the dynamic long-range interactions. We consider the non-Hermitian eigenvalue problem of Eq. (17) with eigenresponse theory. The band structure can be obtained from the peaks of $\max|\alpha_{\text{eig}}|$, and it is shown in Fig. 1(c). Different from the result calculated with quasistatic short-range interactions, we observe a single broadband. The normal modes of the system coupled strongly to the photon mode of the background medium. The band forms outside the light cone with $|k| > \omega/c$, which represent guided modes, and any mode in the light cone with $|k| < \omega/c$ is the radiation mode [51]. There is a blueshift near the Brillouin zone boundary, such that the band is above the resonant frequency of a single gyromagnetic cylinder $\omega_0$. All of these features are different from the results in the quasistatic limit.

To show that the differences are due to the dynamic effects, we consider the system in the quasistatic limit again, but including long-range interactions. Now, we have the eigenvalue problem

$$\boldsymbol{M}'(\boldsymbol{k},\omega)\boldsymbol{m}_i = \lambda_i(\boldsymbol{k},\omega)\boldsymbol{m}_i, \tag{23}$$

where $\boldsymbol{M}'(\boldsymbol{k},\omega)$ is given by Eq. (18). The band structure is shown in Fig. 1(b). We see that, without the dynamic effects, the general features of the band are similar to the blue line, which is the dispersion relation obtained with only short-range interactions, except at the Brillouin zone center $k = 0$, where the group velocity $v_g$ becomes discontinuous.

## III. DIMERIZED CHAIN

### A. Model

To further demonstrate the importance of dynamic long-range interactions in gyromagnetic systems, we consider a dimer model of gyromagnetic cylinders on 1D infinite lattices. In this dimer model, the lattice constant is given by $a_2 = 2a_1 = 18.75$ mm. The unit cell consists of two gyromagnetic cylinders, labeled as $A$ and $B$, with the same radius $r = 2.5$ mm. The displacement from cylinder $A$ to cylinder $B$ is given by $\boldsymbol{b} = b\hat{x}$, with

$$b = \frac{a_2}{2}(1-\delta), \tag{24}$$

where $\delta$ is a dimensionless parameter with $|\delta| \leqslant 0.2$ and hence $b \geqslant 3r$. The system is depicted in Fig. 2(a). The polarizabilities for cylinder $A$ and cylinder $B$ are given by $\boldsymbol{\alpha}_A$ and $\boldsymbol{\alpha}_B$, and their corresponding magnetic dipole moments are given by $\boldsymbol{m}_A$ and $\boldsymbol{m}_B$, respectively. With Bloch's theorem in Eq. (13), the coupled-dipole equations for the dimer model can be written as

$$\begin{pmatrix} \boldsymbol{\alpha}_A^{-1} & 0 \\ 0 & \boldsymbol{\alpha}_B^{-1} \end{pmatrix} \begin{pmatrix} \boldsymbol{m}_A \\ \boldsymbol{m}_B \end{pmatrix} = \boldsymbol{\Gamma} \begin{pmatrix} \boldsymbol{m}_A \\ \boldsymbol{m}_B \end{pmatrix}, \tag{25}$$

with

$$\boldsymbol{\Gamma} := 4\pi k_0^2 \begin{pmatrix} \sum_{\boldsymbol{R}\neq\boldsymbol{0}} \boldsymbol{G}(0,\boldsymbol{R})e^{i\boldsymbol{k}\cdot\boldsymbol{R}} & \sum_{\boldsymbol{R}} \boldsymbol{G}(0,\boldsymbol{R}+\boldsymbol{b})e^{i\boldsymbol{k}\cdot\boldsymbol{R}} \\ \sum_{\boldsymbol{R}} \boldsymbol{G}(0,\boldsymbol{R}-\boldsymbol{b})e^{i\boldsymbol{k}\cdot\boldsymbol{R}} & \sum_{\boldsymbol{R}\neq\boldsymbol{0}} \boldsymbol{G}(0,\boldsymbol{R})e^{i\boldsymbol{k}\cdot\boldsymbol{R}} \end{pmatrix}, \tag{26}$$

and the associated eigenvalue problem with eigenresponse theory is given by

$$\boldsymbol{M}_{\text{dimer}}(\boldsymbol{k},\omega)\boldsymbol{m}_i = \lambda_i(\boldsymbol{k},\omega)\boldsymbol{m}_i, \tag{27}$$

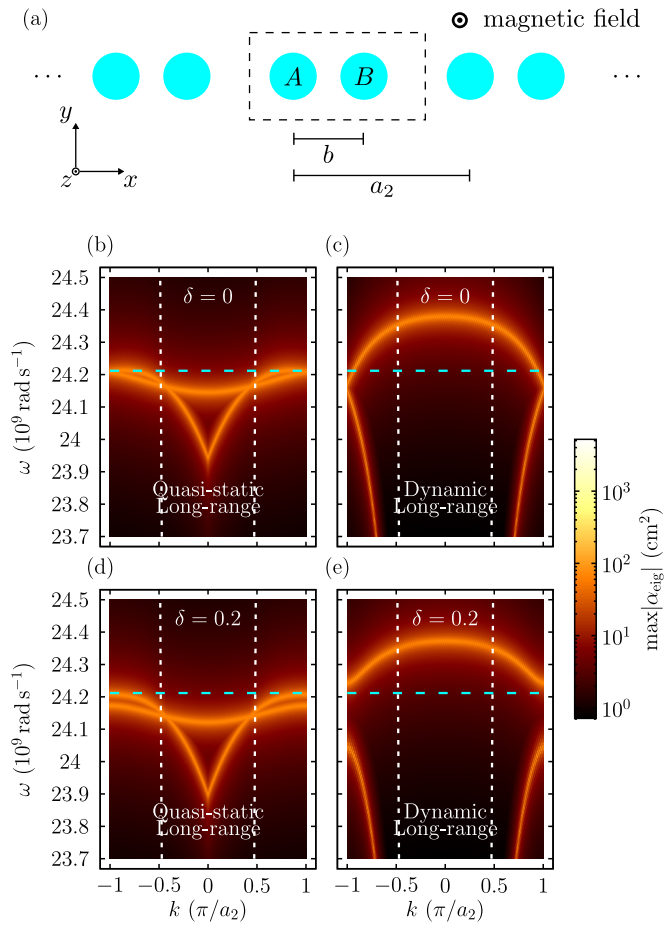


FIG. 2. (a) Illustration of the dimer model of gyromagnetic cylinders on a 1D infinite lattice. The lattice constant is given by $a_2$. The unit cell is indicated by the dashed box. The distance between cylinder $A$ and cylinder $B$ is given by $b = (1-\delta)a_2/2$. (b)–(e) The photonic band structure for the dimer model in the quasistatic limit and in general, with dynamic effects. All results include the long-range interactions. The white dotted lines are the light lines, and the region within the light lines is the light cone. The cyan dashed line indicates the resonant frequency of a single gyromagnetic cylinder $\omega_0$.

where

$$\boldsymbol{M}_{\text{dimer}}(\boldsymbol{k},\omega) := \begin{pmatrix} \boldsymbol{\alpha}_A^{-1} & 0 \\ 0 & \boldsymbol{\alpha}_B^{-1} \end{pmatrix} - \boldsymbol{\Gamma} \tag{28}$$

is a non-Hermitian $4 \times 4$ matrix.

We consider the system with $\delta = 0$ and 0.2, in the quasistatic limit (see Appendix B) and in general, with dynamic effects, all with long-range interactions. Again, the band structure can be obtained from the peaks of $\max|\alpha_{\text{eig}}|$. For $\delta = 0$, the system is the same as that discussed in Sec. II C as depicted in Fig. 1(a). The band structures for this system are shown in Figs. 2(b) and 2(c). Two bands are obtained due to the band folding, and they are physically the same as those in Figs. 1(b) and 1(c). In both cases, the results are gapless and there is degeneracy at the Brillouin zone boundary $k = \pm\pi/a_2$ protected by the inversion symmetry of the system. For the case in the quasistatic limit, this degeneracy is at the resonant frequency of a single gyromagnetic cylinder $\omega_0$, while for the case with dynamic effects it is at a frequency below $\omega_0$.

For $\delta = 0.2$, the band structures are shown in Figs. 2(d) and 2(e). Again, two bands are obtained. For any $\delta \neq 0$, the inversion symmetry of the system is broken, hence the degeneracy split. For the case in the quasistatic limit, the degeneracy at the Brillouin zone boundary $k = \pm\pi/a_2$ is split by one band shifting to a lower frequency, such that the two bands do not exceed the resonant frequency of a single gyromagnetic cylinder $\omega_0$. The system does not have a full band gap, while for the case with dynamic effects the system opens a full band gap. The degeneracy at the Brillouin zone boundary $k = \pm\pi/a_2$ is split, such that the bands are symmetric about the original degeneracy. Moreover, the band gap is larger than that in the quasistatic limit.

We showed that, for a dimer model of gyromagnetic cylinders on a 1D infinite lattice, the system does not have a full band gap in the quasistatic limit, even if long-range interactions are included. Besides breaking inversion symmetry of the system, a full band gap is obtained only when the dynamic long-range interactions are taken into account. This is a major difference with the conventional SSH model and its analogous systems, such as arrays of plasmonic [27,29] and dielectric nanoparticles [33,35]. In plasmonic lattices, although dynamic long-range interactions can also be considered [30–32], studying the system in the quasistatic limit with only short-range interactions is sufficient to obtain a full band gap [27,29,33,35], as long as inversion symmetry is broken in the system. Furthermore, chiral symmetry of the system is broken due to the dynamic long-range interactions [31,32], such that the band structures are not symmetric with respect to the resonant frequency of a single cylinder $\omega_0$. These demonstrated the importance of dynamic long-range interactions on the band structures in gyromagnetic systems.

### B. Topological phase transition

It is known that, for the conventional SSH model, the band topology depends on the distance between the two basis elements in the unit cell [52]. Here, we discuss the topological phase transition in the dimer model of gyromagnetic cylinders on 1D infinite lattices by the associated band inversion [42].

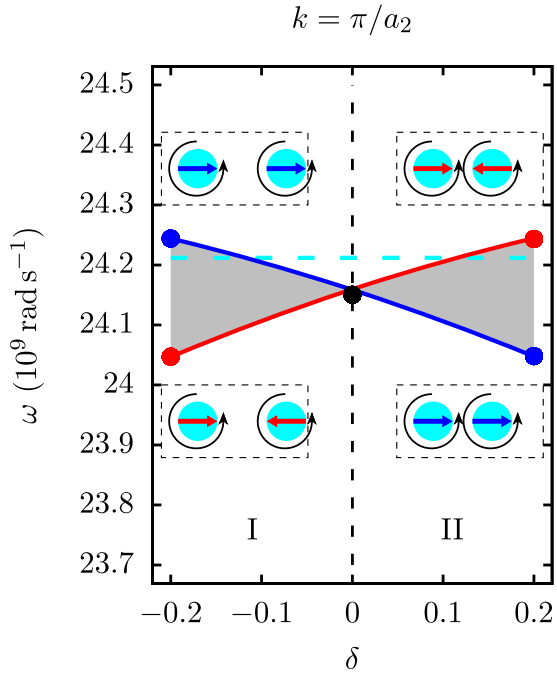


FIG. 3. Band inversion and topological phase transition in the dimer model of gyromagnetic cylinders on a 1D infinite lattice. The curves are the upper and lower band edges at $k = \pi/a_2$ and the gray areas are the band gap. The eigenstates of the unit cell with $\delta = 0.2$ and $-0.2$ for both the upper band and the lower band are illustrated. The in-phase eigenmodes and the corresponding band are in blue, while the antiphase eigenmodes and the corresponding band are in red. The cyan dashed line indicates the resonant frequency of a single gyromagnetic cylinder $\omega_0$. For $\delta < 0$, the system is in topological phase I, while for $\delta > 0$ it is in topological phase II. At $\delta = 0$, the system is gapless, which undergoes band inversion and topological phase transition.

We consider the band structures of the system for $\delta \in [-0.2, 0.2]$ and find the corresponding upper and lower band edges at $k = \pi/a_2$. The results are shown in Fig. 3. The curves are the upper and lower band edges at $k = \pi/a_2$ and the gray areas are the band gaps. The results are symmetric about $\delta = 0$. For $\delta \neq 0$, the system opens a band gap. As $|\delta|$ decrease, the band gap becomes smaller. For $\delta = 0$, the band gap closes, and the system is gapless, which corresponds to the results in Fig. 2(c) at $k = \pi/a_2$. To illustrate the band inversion, we find the eigenmodes of the unit cell with $\delta = 0.2$ and $-0.2$ for both the upper band and the lower band. We see that all the magnetic dipole moments rotate counterclockwise elliptically, as discussed in Sec. II C 1. There are two types of eigenmodes of the unit cell, with a different phase difference $\Delta\theta$ between cylinder $A$ and cylinder $B$: one is in-phase, $\Delta\theta = 0$, and the other is antiphase, $\Delta\theta = \pi$. The in-phase eigenmodes and the corresponding band are in blue, while the antiphase eigenmodes and the corresponding band are in red. It is shown that, as $\delta$ varies and crosses the point $\delta = 0$, the band with in-phase eigenmodes becomes antiphase and vice versa. This observation illustrates band inversion and indicates topological phase transition in the dimer model. For $\delta < 0$, the system is in topological phase I, while for $\delta > 0$ it is

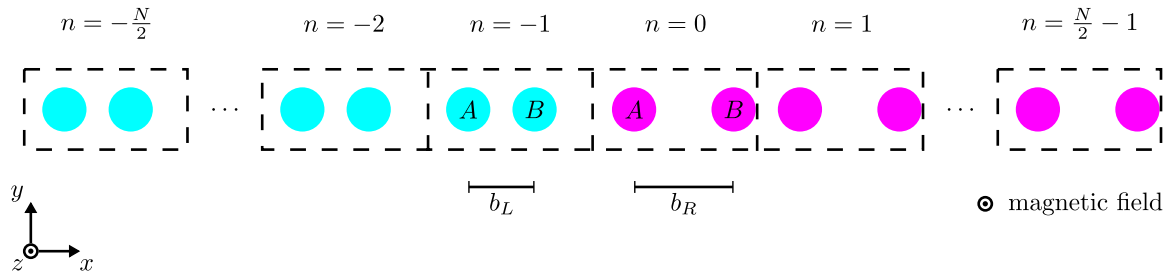


FIG. 4. Illustration of the 1D topological model of gyromagnetic lattices. The lattice constant is given by $a_2$. The finite lattice is composed of a left and a right part with different unit cells. The unit cells are indicated by the dashed boxes and indexed by the integer $n$. The distance between cylinder $A$ and cylinder $B$, in the left and the right part of the lattice, is given by $b_L = (1 - \delta_L)a_2/2$ and $b_R = (1 - \delta_R)a_2/2$, respectively.

in topological phase II. At $\delta = 0$, the system is gapless; it undergoes band inversion and topological phase transition.

### C. Finite lattice and topological edge modes

To demonstrate topological edge modes supporting a 1D gyromagnetic system, we consider a dimer model of gyromagnetic cylinders on a 1D finite lattice in the $x$ direction with lattice constant $a_2 = 18.75$ mm. The finite lattice is composed of a left and a right part with different unit cells. For both the left and the right part of the lattice, the unit cell, indexed by the integer $n$, consists of two gyromagnetic cylinders labeled $A$ and $B$, with the same radius $r = 2.5$ mm as depicted in Fig. 4. We assume there are $N$ unit cells with $N$ being an even number, so $n = -N/2, \ldots, 0, \ldots, N/2 - 1$. Then $n < 0$ corresponds to the left part and $n \geqslant 0$ corresponds to the right part of the lattice. The displacement from cylinder $A$ to $B$ in unit cell $n$ is given by $\boldsymbol{b}_n = b_n\hat{x}$, where

$$b_n = \begin{cases} b_L & \text{if } n < 0, \\ b_R & \text{if } n \geqslant 0, \end{cases} \tag{29}$$

with

$$b_L = \frac{a_2}{2}(1 - \delta_L), \tag{30a}$$

$$b_R = \frac{a_2}{2}(1 - \delta_R). \tag{30b}$$

In the $n$th unit cell, the magnetic dipole moment is $\boldsymbol{m}_n = (\boldsymbol{m}_{n,A}, \boldsymbol{m}_{n,B})^T$ and the polarizability is $\boldsymbol{\alpha}_n(\omega) = \mathrm{diag}(\boldsymbol{\alpha}_{n,A}, \boldsymbol{\alpha}_{n,B})$. Then we have $\tilde{m} = (\boldsymbol{m}_{-N/2}, \ldots, \boldsymbol{m}_0, \ldots, \boldsymbol{m}_{N/2-1})^T$ and $\tilde{\alpha}(\omega) = \mathrm{diag}(\boldsymbol{\alpha}_{-N/2}, \ldots, \boldsymbol{\alpha}_0, \ldots, \boldsymbol{\alpha}_{N/2-1})$. We define $\tilde{\Gamma}(\omega)$ as the interactions between the unit cells $i$ and $j$, such that for $i = j$,

$$\tilde{\Gamma}_{ij} = 4\pi k_0^2 \begin{pmatrix} \mathbf{0} & \boldsymbol{G}(0, \boldsymbol{b}_i) \\ \boldsymbol{G}(0, -\boldsymbol{b}_i) & \mathbf{0} \end{pmatrix}, \tag{31}$$

and for $i \neq j$,

$$\tilde{\Gamma}_{ij} = 4\pi k_0^2 \begin{pmatrix} \boldsymbol{G}(0, \boldsymbol{R}_{ij}) & \boldsymbol{G}(0, \boldsymbol{R}_{ij} + \boldsymbol{b}_i) \\ \boldsymbol{G}(0, \boldsymbol{R}_{ij} - \boldsymbol{b}_i) & \boldsymbol{G}(0, \boldsymbol{R}_{ij}) \end{pmatrix}, \tag{32}$$

where $\boldsymbol{R}_{ij} := (j - i)a_2\hat{x}$ is the displacement from unit cell $i$ to unit cell $j$. Furthermore, we define

$$\tilde{M}_{\mathrm{dimer}}(\omega) := \tilde{\alpha}^{-1}(\omega) - \tilde{\Gamma}(\omega). \tag{33}$$

The coupled-dipole equations for the dimer model of gyromagnetic cylinders on a 1D finite lattice can be written as

$$\tilde{M}_{\mathrm{dimer}}(\omega)\tilde{m} = \mathbf{0}, \tag{34}$$

where $\tilde{M}_{\mathrm{dimer}}(\omega)$ is a $4N \times 4N$ matrix. Finally, we have the eigenvalue problem

$$\tilde{M}_{\mathrm{dimer}}(\omega)\tilde{m}_i = \lambda_i(\omega)\tilde{m}_i, \tag{35}$$

with the eigenresponse theory described in Sec. II B.

We consider the finite lattice with $N = 32$. First, we study the topological trivial case with both $\delta_L = 0.2$ and $\delta_R = 0.2$. This is the finite case of the dimer model studied in Sec. III A with $\delta = 0.2$. To clearly show the eigenmodes, we plot the quantity $\mathrm{Im}(\alpha_{\mathrm{eig}})$. The result is shown in Fig. 5(a). We found that there are two sets of modes corresponding to the upper and the lower band of the system. There is no state within the band gap, as expected. The results are in good agreement with the band structure obtained in Fig. 2(e).

Next, we consider the topological nontrivial case with both $\delta_L = -0.2$ and $\delta_R = -0.2$. As is well known from the conventional SSH model, this system should present topological edge modes at the end of the chain by the bulk-boundary correspondence. The result is shown in Fig. 5(b). Again, we observed that there are two sets of modes corresponding to the upper and the lower band of the system. The bottom of the upper band is labeled by the magenta upper triangle, and the top of the lower band is labeled by the magenta lower triangle. However, in contrast to the trivial case, there is a localized mode on the top of the lower band, which is labeled by the magenta circle. Then we calculated the corresponding norm of the eigenmodes $\|\boldsymbol{m}\| = \sqrt{\boldsymbol{m}^*\boldsymbol{m}}$ of the system. The results for the upper and lower band are shown in Figs. 6(a) and 6(b), respectively. They are the usual normal modes of the system. For the localized mode on the top of the lower band, the norm of the eigenmodes is shown in Fig. 6(c). We see that this eigenmode is localized at $\boldsymbol{m}_{-N/2,A}$ and $\boldsymbol{m}_{N/2-1,B}$, which is at the end of the chain. This is the topological edge mode supporting the system. Since the full band gap in the dimer model only appears when dynamic long-range interactions are included and cannot be predicted by the tight-binding approach, it is very interesting to see that the dynamic long-range interactions lead to localized topological edge modes.

Furthermore, from the results in Fig. 3, we choose the two extreme cases with $\delta_L = 0.2$ and $\delta_R = -0.2$. Then the left part of the lattice is in topological phase II, while

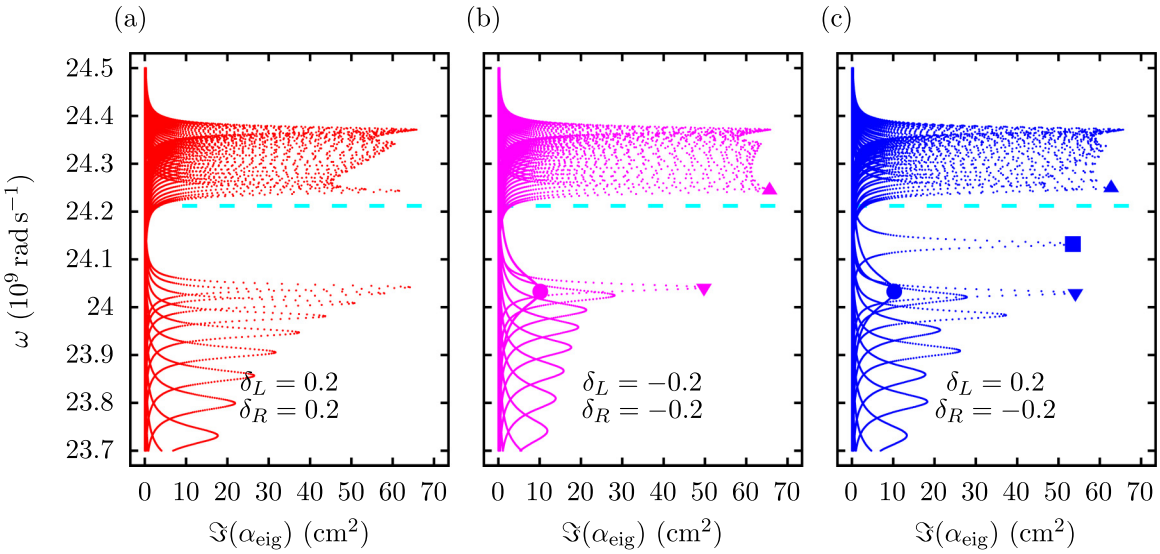


FIG. 5. Band structures of the dimer model of gyromagnetic cylinders on a 1D finite lattice. (a) The topologically trivial system with both $\delta_L = 0.2$ and $\delta_R = 0.2$. (b) The topologically nontrivial system with both $\delta_L = -0.2$ and $\delta_R = -0.2$. (c) The system with $\delta_L = 0.2$ and $\delta_R = -0.2$, where the left and the right parts of the lattice are topologically trivial and nontrivial, respectively. The upper and the lower triangle indicate the upper and the lower bands, respectively. The circle and the square are the topological edge modes. The cyan dashed line indicates the resonant frequency of a single gyromagnetic cylinder $\omega_0$.

the right part of the lattice is in topological phase I. The result is shown in Fig. 5(c). Again, we observed the upper and the lower band of the system, which are labeled by the upper blue triangle and the lower blue triangle, respectively. Besides the localized mode on the top of the lower band, which is labeled by the blue circle, there is also a localized mode at the center of the band gap, which is labeled by the blue square. There are two topological edge modes supporting this system. The corresponding eigenmodes for the upper and the lower band are shown in Figs. 6(d) and 6(g), respectively. The eigenmodes are neither symmetric nor antisymmetric about the center of the chain because the system has a broken

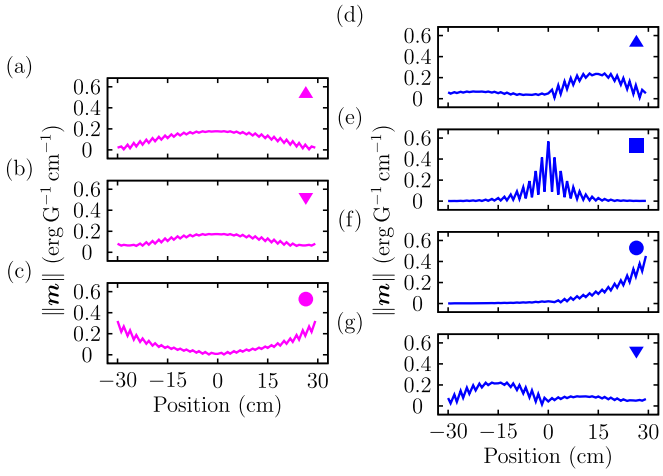


FIG. 6. The norm of eigenmodes corresponding to the labeled modes in the band structures in Fig. 5. (a)–(c) The results for the system with $\delta_L = -0.2$ and $\delta_R = -0.2$. (d)–(g) The results for the system with $\delta_L = 0.2$ and $\delta_R = -0.2$. In particular, (c), (e), and (f) are topological edge modes.

inversion and reflection symmetry. For the localized mode on the top of the lower band, the norm of the eigenmode is shown in Fig. 6(f). Now, this eigenmode is only localized at $\boldsymbol{m}_{N/2-1,B}$, which is the right end of the chain. For the localized mode at the center of the band gap, the norm of the eigenmode is shown in Fig. 6(e). It is shown that this eigenmode is localized at $\boldsymbol{m}_{0,A}$, which is the boundary between the left and the right part of the lattice. As long as the left part and the right part of the lattice are in two distinct topological phases, protected modes exist at the boundary where there is a topological phase transition.

To study the effects of dynamic long-range interactions on the topological edge modes, we consider the system with fixed $\delta_L = 0.2$ and $\delta_R \in [-0.2, 0.2]$. The band structures are shown in Fig. 7. For $\delta_R > 0$, both the left and the right part of the lattice are in the same topological phase II. As a result, there is no mode within the band gap in the system. We observed that, as $\delta_R$ decreases from $\delta_R = 0.2$, the band gap becomes smaller. When the system crosses $\delta_R = 0$, which is indicated by the white dashed line, the right part of the lattice undergoes a topological phase transition, as discussed in Sec. III B. Hence, for $\delta_R < 0$, the right part of the lattice is in topological phase I. Now, the left and the right part of the lattice are in two distinct topological phases. By the prediction of the bulk-boundary correspondence, topological edge modes will exist. We observed that, after the system crossing $\delta_R = 0$, the topological edge mode emerges from the bottom of the upper band and it is redshifted from the resonant frequency of a single gyromagnetic cylinder $\omega_0$.

In the conventional SSH model and its analogous systems, the topological edge modes can be predicted by the bulk-boundary correspondence with a tight-binding approach in the quasistatic limit, where only nearest-neighbor interactions are being considered. However, this is not possible with our 1D topological model for a gyromagnetic system. As seen in

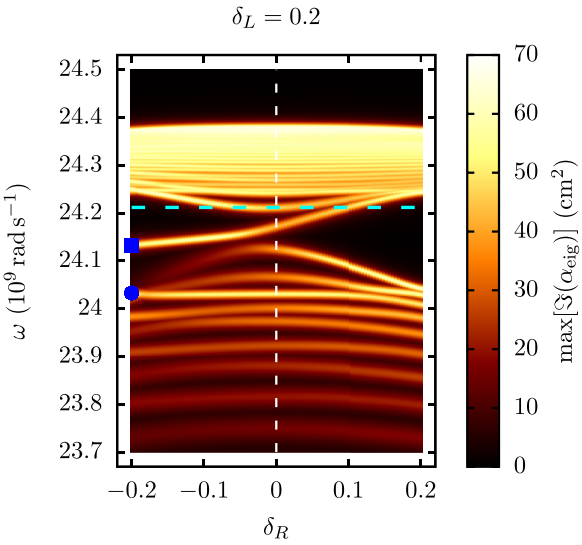


FIG. 7. Topological phase transition of the dimer model of gyromagnetic cylinders on a 1D finite lattice with $\delta_L = 0.2$ and $\delta_R \in [-0.2, 0.2]$. The white dashed line at $\delta_R = 0$ indicates topological phase transition in the right part of the lattice, and the cyan dashed line indicates the resonant frequency of a single gyromagnetic cylinder $\omega_0$. The blue square and the blue circle are the topological edge modes.

Fig. 2(d), in the quasistatic limit, apart from not having a full band gap, the resonant frequency of a single gyromagnetic cylinder $\omega_0$, which corresponds to the zero-energy state in the SSH model, is on top of the bands. Since the chiral symmetry ensures that the spectral position of any edge mode lies at $\omega_0$, the topological nature of the edge mode is not well defined. As discussed in Sec. III A, in order to obtain a full band gap, the dynamic long-range interactions have to be taken into account. Furthermore, the chiral symmetry of the system is broken due to the dynamic long-range interactions [31,32], and the topological edge modes are redshifted from $\omega_0$, such that they are within two topological bands and can be understood by the bulk-boundary correspondence. Therefore, the dynamic long-range interaction plays a crucial role in opening a band gap and supporting the topological edge modes in our system. Part of the band structures and edge modes (or density of states) of this topological 1D array of gyromagnetic cylinders could be verified experimentally through measurement of the transmission along the chain using near-field techniques [53–56].

## IV. CONCLUSION

In conclusion, we studied the dynamic long range interaction induced topological photonic edge modes in a one-dimensional (1D) array of strongly dispersive gyromagnetic resonant cylinders. In the case of dimer lattices, we found that the creation of the nontrivial band gaps and topological edge modes relies on the dynamic long range interaction associated with the free-space photon modes of the background medium. Our results indicate that the dynamic long range interaction plays a crucial role in predicting the precise band structures and the spectral position of the topological edge modes in gyromagnetic systems.

## ACKNOWLEDGMENTS

This work was supported by the Research Grant Council of Hong Kong through the General Research Fund (15300315, 15301917) and the Area of Excellence Scheme (AoE/P-02/12). Support from The Hong Kong Polytechnic University (through B-Q58F) should be acknowledged. The authors would also like to thank C. W. Ling, Ka Hei Choi, C. T. Chan, Wai Chun Wong, and Wang Tat Yau for useful discussions.

## APPENDIX A: COUPLED-DIPOLE EQUATIONS IN THE QUASISTATIC LIMIT

In the quasistatic limit $k_0 \to 0$, the Hankel functions in Eq. (7) become [57]

$$H_0^{(1)}(k_0 R) \sim \frac{2i}{\pi} \ln k_0 R, \tag{A1a}$$

$$H_1^{(1)}(k_0 R) \sim -\frac{2i}{\pi}\left(\frac{1}{k_0 R}\right). \tag{A1b}$$

Hence, the 2D Green's tensor for our system in the quasistatic limit is given by

$$\boldsymbol{G}'(\boldsymbol{\rho}, \boldsymbol{\rho}') = \begin{pmatrix} G'_{xx} & 0 \\ 0 & G'_{yy} \end{pmatrix}, \tag{A2}$$

with

$$G_{xx} = \frac{1}{2\pi}\frac{1}{(k_0 R)^2}, \tag{A3a}$$

$$G_{yy} = -\frac{1}{2\pi}\left(\ln k_0 R + \frac{1}{(k_0 R)^2}\right). \tag{A3b}$$

Now, $\boldsymbol{G}'$ is real symmetric. Moreover, we define

$$\boldsymbol{A}(\boldsymbol{\rho}, \boldsymbol{\rho}') := \lim_{k_0 \to 0} 4\pi k_0^2 \boldsymbol{G}'(\boldsymbol{\rho}, \boldsymbol{\rho}'), \tag{A4}$$

and since $\lim_{k_0 \to 0} k_0^2 \ln k_0 R = 0$,

$$\boldsymbol{A}(\boldsymbol{\rho}, \boldsymbol{\rho}') = \begin{pmatrix} \frac{2}{R^2} & 0 \\ 0 & -\frac{2}{R^2} \end{pmatrix}. \tag{A5}$$

The polarizability in the quasistatic limit $\boldsymbol{\alpha}'(\omega)$ is obtained by eliminating the radiative correction term in Eq. (1), as $\lim_{k_0 \to 0} -i(\pi k_0^2/2)\boldsymbol{I} = \boldsymbol{0}$. We have

$$\boldsymbol{\alpha}'^{-1}(\omega) = \frac{4}{r^2}\begin{pmatrix} \frac{\omega_h}{\omega_m} + \frac{1}{2} - i\beta\frac{\omega}{\omega_m} & i\frac{\omega}{\omega_m} \\ -i\frac{\omega}{\omega_m} & \frac{\omega_h}{\omega_m} + \frac{1}{2} - i\beta\frac{\omega}{\omega_m} \end{pmatrix}. \tag{A6}$$

Then the coupled-dipole equations in the quasistatic limit are given by

$$\boldsymbol{m}(\boldsymbol{\rho}) = \boldsymbol{\alpha}'(\omega)\left(\sum_{\boldsymbol{\rho}' \neq \boldsymbol{\rho}} \boldsymbol{A}(\boldsymbol{\rho}, \boldsymbol{\rho}')\boldsymbol{m}(\boldsymbol{\rho}') + \boldsymbol{B}_0(\boldsymbol{\rho})\right), \tag{A7}$$

and in the formalism of eigenresponse theory, we define

$$\boldsymbol{M}'(\omega) := \boldsymbol{\alpha}'^{-1}(\omega) - \sum_{\boldsymbol{\rho}' \neq \boldsymbol{\rho}} \boldsymbol{A}(\boldsymbol{\rho}, \boldsymbol{\rho}'). \tag{A8}$$

For an infinite lattice, with Bloch's theorem in Eq. (13), Eq. (A7) becomes

$$\boldsymbol{m}(\boldsymbol{\rho}) = \boldsymbol{\alpha}'(\omega)\left(\sum_{\boldsymbol{R}\neq 0}\boldsymbol{A}(0,\boldsymbol{R})e^{i\boldsymbol{k}\cdot\boldsymbol{R}}\boldsymbol{m}(\boldsymbol{\rho}') + \boldsymbol{B}_0(\boldsymbol{\rho})\right). \tag{A9}$$

Then we define

$$\boldsymbol{M}'(\boldsymbol{k},\omega) := \boldsymbol{\alpha}'^{-1}(\omega) - \sum_{\boldsymbol{R}\neq 0}\boldsymbol{A}(0,\boldsymbol{R})e^{i\boldsymbol{k}\cdot\boldsymbol{R}}. \tag{A10}$$

It should be noted that, although $\boldsymbol{A}$ is real symmetric, $\boldsymbol{\alpha}'$ is non-Hermitian, so $\boldsymbol{M}'$ in both Eqs. (A8) and (A10) are also non-Hermitian.

## APPENDIX B: COUPLED-DIPOLE EQUATIONS FOR THE DIMER MODEL IN THE QUASISTATIC LIMIT

We consider the dimer model in Sec. III A in the quasistatic limit, $k_0 \to 0$. The polarizabilities for cylinder $A$ and cylinder $B$ are given by Eq. (A6) and are denoted by $\boldsymbol{\alpha}'_A$ and $\boldsymbol{\alpha}'_B$, respectively. With Bloch's theorem in Eq. (13) and with Eq. (A5), the coupled-dipole equations for the dimer model can be written as

$$\begin{pmatrix}\boldsymbol{\alpha}'^{-1}_A & 0\\ 0 & \boldsymbol{\alpha}'^{-1}_B\end{pmatrix}\begin{pmatrix}\boldsymbol{m}_A\\ \boldsymbol{m}_B\end{pmatrix} = \boldsymbol{\Gamma}'\begin{pmatrix}\boldsymbol{m}_A\\ \boldsymbol{m}_B\end{pmatrix}, \tag{B1}$$

where we have defined

$$\boldsymbol{\Gamma}' := \begin{pmatrix}\sum\limits_{\boldsymbol{R}\neq 0}\boldsymbol{A}(0,\boldsymbol{R})e^{i\boldsymbol{k}\cdot\boldsymbol{R}} & \sum\limits_{\boldsymbol{R}}\boldsymbol{A}(0,\boldsymbol{R}+\boldsymbol{b})e^{i\boldsymbol{k}\cdot\boldsymbol{R}}\\ \sum\limits_{\boldsymbol{R}}\boldsymbol{A}(0,\boldsymbol{R}-\boldsymbol{b})e^{i\boldsymbol{k}\cdot\boldsymbol{R}} & \sum\limits_{\boldsymbol{R}\neq 0}\boldsymbol{A}(0,\boldsymbol{R})e^{i\boldsymbol{k}\cdot\boldsymbol{R}}\end{pmatrix}. \tag{B2}$$

It should be noted that, since $\boldsymbol{A}$ is real symmetric, $\boldsymbol{\Gamma}'$ is Hermitian. In the formalism of eigenresponse theory, we define

$$\boldsymbol{M}'_{\text{dimer}}(\boldsymbol{k},\omega) := \begin{pmatrix}\boldsymbol{\alpha}'^{-1}_A & 0\\ 0 & \boldsymbol{\alpha}'^{-1}_B\end{pmatrix} - \boldsymbol{\Gamma}'. \tag{B3}$$

Now, since $\boldsymbol{\alpha}'$ is non-Hermitian, $\boldsymbol{M}'$ is also non-Hermitian.


[1] L. Lu, J. D. Joannopoulos, and M. Soljačić, Topological photonics, Nat. Photon. **8**, 821 (2014).

[2] T. Ozawa, H. M. Price, A. Amo, N. Goldman, M. Hafezi, L. Lu, M. C. Rechtsman, D. Schuster, J. Simon, O. Zilberberg, and I. Carusotto, Topological photonics, Rev. Mod. Phys. **91**, 015006 (2019).

[3] F. D. M. Haldane and S. Raghu, Possible Realization of Directional Optical Waveguides in Photonic Crystals with Broken Time-Reversal Symmetry, Phys. Rev. Lett. **100**, 013904 (2008).

[4] Z. Wang, Y. D. Chong, J. D. Joannopoulos, and M. Soljačić, Reflection-Free One-Way Edge Modes in a Gyromagnetic Photonic Crystal, Phys. Rev. Lett. **100**, 013905 (2008).

[5] S. Raghu and F. D. M. Haldane, Analogs of quantum-Hall-effect edge states in photonic crystals, Phys. Rev. A **78**, 033834 (2008).

[6] Z. Wang, Y. Chong, J. D. Joannopoulos, and M. Soljačić, Observation of unidirectional backscattering-immune topological electromagnetic states, Nature (London) **461**, 772 (2009).

[7] K. Fang, Z. Yu, and S. Fan, Microscopic theory of photonic one-way edge mode, Phys. Rev. B **84**, 075477 (2011).

[8] M. Hafezi, E. A. Demler, M. D. Lukin, and J. M. Taylor, Robust optical delay lines with topological protection, Nat. Phys. **7**, 907 (2011).

[9] M. Hafezi, S. Mittal, J. Fan, A. Migdall, and J. Taylor, Imaging topological edge states in silicon photonics, Nat. Photon. **7**, 1001 (2013).

[10] A. B. Khanikaev, S. H. Mousavi, W.-K. Tse, M. Kargarian, A. H. MacDonald, and G. Shvets, Photonic topological insulators, Nat. Mater. **12**, 233 (2013).

[11] L.-H. Wu and X. Hu, Scheme for Achieving a Topological Photonic Crystal by Using Dielectric Material, Phys. Rev. Lett. **114**, 223901 (2015).

[12] J. Ningyuan, C. Owens, A. Sommer, D. Schuster, and J. Simon, Time- and Site-Resolved Dynamics in a Topological Circuit, Phys. Rev. X **5**, 021031 (2015).

[13] B. M. Anderson, R. Ma, C. Owens, D. I. Schuster, and J. Simon, Engineering Topological Many-Body Materials in Microwave Cavity Arrays, Phys. Rev. X **6**, 041043 (2016).

[14] C. Owens, A. LaChapelle, B. Saxberg, B. M. Anderson, R. Ma, J. Simon, and D. I. Schuster, Quarter-flux Hofstadter lattice in a qubit-compatible microwave cavity array, Phys. Rev. A **97**, 013818 (2018).

[15] L. Lu, L. Fu, J. D. Joannopoulos, and M. Soljačić, Weyl points and line nodes in gyroid photonic crystals, Nat. Photon. **7**, 294 (2013).

[16] X.-W. Luo, X. Zhou, C.-F. Li, J.-S. Xu, G.-C. Guo, and Z.-W. Zhou, Quantum simulation of 2d topological physics in a 1d array of optical cavities, Nat. Commun. **6**, 7704 (2015).

[17] O. Zilberberg, S. Huang, J. Guglielmon, M. Wang, K. P. Chen, Y. E. Kraus, and M. C. Rechtsman, Photonic topological boundary pumping as a probe of 4d quantum hall physics, Nature (London) **553**, 59 (2018).

[18] P. St-Jean, V. Goblot, E. Galopin, A. Lemaître, T. Ozawa, L. Le Gratiet, I. Sagnes, J. Bloch, and A. Amo, Lasing in topological edge states of a one-dimensional lattice, Nat. Photon. **11**, 651 (2017).

[19] B. Bahari, A. Ndao, F. Vallini, A. El Amili, Y. Fainman, and B. Kanté, Nonreciprocal lasing in topological cavities of arbitrary geometries, Science **358**, 636 (2017).

[20] H. Zhao, P. Miao, M. H. Teimourpour, S. Malzard, R. El-Ganainy, H. Schomerus, and L. Feng, Topological hybrid silicon microlasers, Nat. Commun. **9**, 981 (2018).

[21] M. Parto, S. Wittek, H. Hodaei, G. Harari, M. A. Bandres, J. Ren, M. C. Rechtsman, M. Segev, D. N. Christodoulides, and M. Khajavikhan, Edge-Mode Lasing in 1D Topological Active Arrays, Phys. Rev. Lett. **120**, 113901 (2018).

[22] G. Harari, M. A. Bandres, Y. Lumer, M. C. Rechtsman, Y. D. Chong, M. Khajavikhan, D. N. Christodoulides, and M. Segev, Topological insulator laser: Theory, Science **359**, eaar4003 (2018).

[23] M. A. Bandres, S. Wittek, G. Harari, M. Parto, J. Ren, M. Segev, D. N. Christodoulides, and M. Khajavikhan, Topological insulator laser: Experiments, Science **359**, eaar4005 (2018).

[24] R. Keil, J. M. Zeuner, F. Dreisow, M. Heinrich, A. Tünnermann, S. Nolte, and A. Szameit, The random mass dirac model and long-range correlations on an integrated optical platform, Nat. Commun. **4**, 1368 (2013).

[25] M. Xiao, Z. Q. Zhang, and C. T. Chan, Surface Impedance and Bulk Band Geometric Phases in One-Dimensional Systems, Phys. Rev. X **4**, 021017 (2014).

[26] A. Poddubny, A. Miroshnichenko, A. Slobozhanyuk, and Y. Kivshar, Topological majorana states in zigzag chains of plasmonic nanoparticles, ACS Photon. **1**, 101 (2014).

[27] C. W. Ling, M. Xiao, C. T. Chan, S. F. Yu, and K. H. Fung, Topological edge plasmon modes between diatomic chains of plasmonic nanoparticles, Opt. Express **23**, 2021 (2015).

[28] I. S. Sinev, I. S. Mukhin, A. P. Slobozhanyuk, A. N. Poddubny, A. E. Miroshnichenko, A. K. Samusev, and Y. S. Kivshar, Mapping plasmonic topological states at the nanoscale, Nanoscale **7**, 11904 (2015).

[29] C. A. Downing and G. Weick, Topological collective plasmons in bipartite chains of metallic nanoparticles, Phys. Rev. B **95**, 125426 (2017).

[30] Y.-L. Zhang, R. P. H. Wu, A. Kumar, T. Si, and K. H. Fung, Nonsymmorphic symmetry-protected topological modes in plasmonic nanoribbon lattices, Phys. Rev. B **97**, 144203 (2018).

[31] S. R. Pocock, X. Xiao, P. A. Huidobro, and V. Giannini, Topological plasmonic chain with retardation and radiative effects, ACS Photon. **5**, 2271 (2018).

[32] C. A. Downing and G. Weick, Topological plasmons in dimerized chains of nanoparticles: Robustness against long-range quasistatic interactions and retardation effects, Eur. Phys. J. B **91**, 253 (2018).

[33] A. P. Slobozhanyuk, A. N. Poddubny, A. E. Miroshnichenko, P. A. Belov, and Y. S. Kivshar, Subwavelength Topological Edge States in Optically Resonant Dielectric Structures, Phys. Rev. Lett. **114**, 123901 (2015).

[34] A. P. Slobozhanyuk, A. N. Poddubny, I. S. Sinev, A. K. Samusev, Y. F. Yu, A. I. Kuznetsov, A. E. Miroshnichenko, and Y. S. Kivshar, Enhanced photonic spin hall effect with subwavelength topological edge states, Laser Photon. Rev. **10**, 656 (2016).

[35] S. Kruk, A. Slobozhanyuk, D. Denkova, A. Poddubny, I. Kravchenko, A. Miroshnichenko, D. Neshev, and Y. Kivshar, Edge states and topological phase transitions in chains of dielectric nanoparticles, Small **13**, 1603190 (2017).

[36] W. P. Su, J. R. Schrieffer, and A. J. Heeger, Solitons in Polyacetylene, Phys. Rev. Lett. **42**, 1698 (1979).

[37] J. K. Asbóth, L. Oroszlány, and A. Pályi, The Su-Schrieffer-Heeger (SSH) model, in *A Short Course on Topological Insulators: Band Structure and Edge States in One and Two Dimensions*, Lecture Notes in Physics Vol. 919 (Springer, Cham, 2016), pp. 1–22.

[38] D. J. Bergman and D. Stroud, Theory of resonances in the electromagnetic scattering by macroscopic bodies, Phys. Rev. B **22**, 3527 (1980).

[39] V. A. Markel, Antisymmetrical optical states, J. Opt. Soc. Am. B **12**, 1783 (1995).

[40] K. H. Fung and C. T. Chan, Plasmonic modes in periodic metal nanoparticle chains: A direct dynamic eigenmode analysis, Opt. Lett. **32**, 973 (2007).

[41] K. H. Fung and C. T. Chan, Analytical study of the plasmonic modes of a metal nanoparticle circular array, Phys. Rev. B **77**, 205423 (2008).

[42] M. Xiao, G. Ma, Z. Yang, P. Sheng, Z. Zhang, and C. T. Chan, Geometric phase and band inversion in periodic acoustic systems, Nat. Phys. **11**, 240 (2015).

[43] W. H. Weber and G. W. Ford, Propagation of optical excitations by dipolar interactions in metal nanoparticle chains, Phys. Rev. B **70**, 125429 (2004).

[44] P. C. Chaumet and M. Nieto-Vesperinas, Coupled dipole method determination of the electromagnetic force on a particle over a flat dielectric substrate, Phys. Rev. B **61**, 14119 (2000).

[45] D. M. Bolle and L. Lewin, On the definitions of parameters in ferrite-electromagnetic wave interactions (letters), IEEE Trans. Microwave Theor. Technol. **21**, 118 (1973).

[46] X. Ao, Z. Lin, and C. T. Chan, One-way edge mode in a magneto-optical honeycomb photonic crystal, Phys. Rev. B **80**, 033105 (2009).

[47] A. A. Asatryan, L. C. Botten, K. Fang, S. Fan, and R. C. McPhedran, Local density of states of chiral Hall edge states in gyrotropic photonic clusters, Phys. Rev. B **88**, 035127 (2013).

[48] D. M. Pozar, Theory and design of ferrimagnetic components, in *Microwave Engineering*, 4th ed. (Wiley, Hoboken, 2009), pp. 451–495.

[49] L. Novotny and B. Hecht, Theoretical foundations, in *Principles of Nano-Optics*, 2nd ed. (Cambridge University Press, Cambridge, 2012), p. 12.

[50] O. J. F. Martin and N. B. Piller, Electromagnetic scattering in polarizable backgrounds, Phys. Rev. E **58**, 3909 (1998).

[51] J. D. Joannopoulos, S. G. Johnson, J. N. Winn, and R. D. Meade, Symmetries and solid-state electromagnetism, in *Photonic Crystals: Molding the Flow of Light*, 2nd ed. (Princeton University Press, Princeton, NJ, 2008), pp. 25–43.

[52] M. Atala, M. Aidelsburger, J. T. Barreiro, D. Abanin, T. Kitagawa, E. Demler, and I. Bloch, Direct measurement of the zak phase in topological bloch bands, Nat. Phys. **9**, 795 (2013).

[53] S. L. McCall, P. M. Platzman, R. Dalichaouch, D. Smith, and S. Schultz, Microwave Propagation in Two-Dimensional Dielectric Lattices, Phys. Rev. Lett. **67**, 2017 (1991).

[54] W. M. Robertson, G. Arjavalingam, R. D. Meade, K. D. Brommer, A. M. Rappe, and J. D. Joannopoulos, Measurement of Photonic Band Structure in a Two-Dimensional Periodic Dielectric Array, Phys. Rev. Lett. **68**, 2023 (1992).

[55] Q. Cheng, X. Yang, H. Ma, J. Chin, T. Cui, R. Liu, and D. Smith, Experiments and applications of metamaterials in microwave regime, in *Metamaterials* (Springer, New York, 2010), pp. 321–355.

[56] Z. Li, R. Xin Wu, Q. Bo Li, and Y. Poo, Realization of self-guided unidirectional waveguides by a chain of gyromagnetic rods, Appl. Opt. **54**, 1267 (2015).

[57] M. L. Boas, Series solutions of differential equations; Legendre, Bessel, Hermite, and Laguerre functions, in *Mathematical Methods in the Physical Sciences*, 3rd ed. (Wiley, Hoboken, 2006), pp. 562–618.